JOURNAL OF COMPUTATIONAL PHYSICS 22, 295–318 (1976)

# The Application of the Second and Third Degree Methods

J. STEPPELER

*Deutscher Wetterdienst, Zentralamt, Frankfurter Strasse 135, Offenbach, West Germany*

Received February 3, 1976; revised May 10, 1976

Further examples are given of a finite difference scheme which was introduced in a previous paper. The aim of these examples is to show the possibility of practical applications. The accuracy obtainable is demonstrated by the solution of a linear equation. The vortex behind a barrier and a physical instability case (Helmholtz instability) are computed to show the nonlinear stability of the scheme.

## 1. INTRODUCTION

In a previous paper [1] a finite difference scheme for accurately solving partial differential equations was introduced. The accuracy achieved was associated with the degree parameter of the method. In [1] the presentation was confined to the first and second degree cases and to one space dimension. Now, more general examples are given.

The aim of these examples is to show the possibility of practical applications. From this point of view the $\rho$th degree method has two advantages:

(a) For a given scale, any desired accuracy can be achieved with a reasonable computational effort.

(b) Nonlinear stability is maintained with a moderate damping of the larger scales.

To support (a) the linear analysis of the third degree method will be given. It reveals a further increase of accuracy compared with the second degree method.

The effect of nonlinear instability is physically related to the fact that a phenomenon can change its scale during time development. This poses a hard test for a finite difference scheme, when the waves that arise cannot be represented in the grid. A finite difference scheme must not necessarily fail to give reasonable results under these circumstances. An example is the pseudoviscosity method of computing shocks [3]. The idea is to smooth the shock to a scale which can be represented by the grid. In the same way, the second degree method disposes of short waves.

The difference of the modes with small and heavy damping is very marked for the second degree method, and still more marked for the third degree method.

For computations in two space dimensions, physical situations were selected which require schemes with good nonlinear stability properties.

To avoid unnecessary complications in presentation, no attempt was made to describe a fairly general case of the method. Instead, specific examples in one and two space dimensions are given. Some care is taken to describe the mathematical ideas involved. Further generalizations should now be straightforward. These generalizations may concern the following points.

(a) The definition of the method for arbitrary degree and space dimension,

(b) the choice of other spatial smoothing operations,

(c) the definition of an implicit or semi-implicit version of the $\rho$th degree method.

The investigation of (b) seems especially interesting since numerical experiments have shown that the choice of the spatial smoothing operation has an essential influence on the Courant–Levy timestep and other features of the resulting scheme. It does not seem likely that the operation described in this paper is the best choice for all possible applications.

The formalism is given in Section 2. Section 3 describes numerical computations which demonstrate the accuracy and nonlinear stability of the schemes.

## 2. Definitions

*One Space Dimension*

Equations of the form

$$(\partial/\partial t)\mathbf{r} = F(\mathbf{r}, D\mathbf{r}) \tag{1}$$

are considered, where $D$ is a spatial differential operator of order smaller than 4.

As in [1] we will use the grid $X_\nu$ with $\Delta X = X_{\nu+1} - X_\nu$ and the shifted grid $X_\nu' = (X_{\nu+1} + X_\nu)/2$. For the definition of the third degree scheme the function spaces $S_3$, $P_3$, $S_3'$, $P_3'$ will be used. At a fixed time level $t$ the fields will be given as functions belonging to $S_3$ or $S_3'$ in the original and the shifted grid, respectively. Functions from $P_3$ or $P_3'$ will occur when the time translation operator is applied to functions from $S_3$ or $S_3'$, respectively. For simplicity the definition of these spaces will be given for the periodic boundary case with periodicity length $L\Delta X$. All series $\alpha_\nu$ used in the future are required to be periodic:

$$\alpha_{\nu+L} = \alpha_\nu .$$

For the definition of a function $\phi(X) \in S_3$ the constants $\phi_\nu$, $\phi_{\nu+(1/2),X2}$, $\phi_{\nu+(1/2),X3}$ must be given. These constants correspond to gridpoint values of $\phi$ and second and third spatial derivatives at intermediate points.

For $X \in [X_\nu, X_{\nu+1}]$ $\phi(x)$ is defined by

$$\phi(x) = ((\phi_{\nu+1} + \phi_\nu)/2) + ((\phi_{\nu+1} - \phi_\nu)/\Delta X) \cdot (X - X_{\nu+(1/2)}) + \phi_{\nu+(1/2),X2} f_2(X - X_{\nu+(1/2)}) + \phi_{\nu+(1/2),X3} f_3(X - X_{\nu+(1/2)}) \quad (2)$$

with $f_2(Y) = (Y^2 - \Delta X^2/4)/2$ and $f_3(Y) = (Y/3) f_2(Y)$.

For the definition of a function $\bar{\phi} \in P_3$ let the coefficients $\bar{\phi}_{\nu+(1/2),0}$; $\bar{\phi}_{\nu+(1/2),X}$; $\bar{\phi}_{\nu+(1/2),XX}$; $\bar{\phi}_{\nu+(1/2),XXX}$ be given. They are the coefficients of a spatial Taylor series of $\bar{\phi}$. For $X \in [X_\nu, X_{\nu+1}]$ $\bar{\phi}(X)$ is defined by

$$\bar{\phi}(X) = \bar{\phi}_{\nu+(1/2),0} + \bar{\phi}_{\nu+(1/2),X}(X - X_{\nu+(1/2)}) + \bar{\phi}_{\nu+(1/2),XX}(X - X_{\nu+(1/2)})^2/2 + \bar{\phi}_{\nu+(1/2),XXX}(X - X_{\nu+(1/2)})^3/6. \quad (3)$$

The functions $\phi'(X) \in S_3'$ and $\bar{\phi}'(X) \in P_3'$ are defined by applying shifting operations to functions $\phi(X) \in S_3$ or $\bar{\phi}(X) \in P_3$, respectively:

$$\phi'(X) = \phi(X + \Delta X/2), \qquad \bar{\phi}'(X) = \bar{\phi}(X + \Delta X/2).$$

The spaces $S_3$ and $S_3'$ consist of continuous functions, while the elements of $P_3$ and $P_3'$ may have discontinuities at $X_\nu$ or $X_\nu'$, respectively.

The time translation operator $T_{\Delta t}$ is defined on the space $B_A$. $B_A$ consists of all functions $\psi(X)$ which are analytic on the interval $[0, L\Delta X]$, except possibly at a finite number of points, and satisfy the periodicity condition

$$\psi(X) = \psi(X + L\Delta X).$$

$T_{\Delta t}$ is defined by

$$T_{\Delta t}\psi(X) = \psi(X) + \sum_{n=1}^{\rho} \psi^{(n)}(X)(\Delta t^n/n!) \quad (4)$$

for the $\rho$th degree case. The equation of motion, Eq. (1), determines all coefficients $\psi^{(n)}(X)$ if we assume that the left-hand side of Eq. (4) with $\rho = \infty$ is a solution.

As in [1], spatial smoothing operations $Q$, $Q'$ will be needed which map $P_3$ to $S_3'$ and $P_3'$ to $S_3$, respectively. For the definition of $Q$ let a function $\bar{\phi} \in P_3$ be given, with corresponding constants $\bar{\phi}_{\nu+(1/2),0}$; $\bar{\phi}_{\nu+(1/2),X}$; $\bar{\phi}_{\nu+(1/2),XX}$; $\bar{\phi}_{\nu+(1/2),XXX}$. The constants $\phi'_{\nu+(1/2)}$; $\phi'_{\nu,X2}$; $\phi'_{\nu,X3}$ defining the function $Q\bar{\phi} = \phi' \in S_3'$ are determined by the equations

$$\begin{aligned} \phi'_{\nu+(1/2)} &= \bar{\phi}(X_{\nu+(1/2)}), \\ (\partial/\partial\phi'_{\nu,X2}) \| \phi' - \bar{\phi} \|^2_{1,\nu} &= 0, \\ (\partial/\partial\xi\phi'_{\nu,X3}) \| \phi' - \bar{\phi} \|^2_{2,\nu} &= 0. \end{aligned} \quad (5)$$

The parameter $\xi$ is used to control the implicit spatial smoothing of the method. In the following the value $\xi = 1.1$ will be used. In Eqs. (5), $\| \ \|_{1,\nu}$ and $\| \ \|_{2,\nu}$ are norms defined on a space containing $S_3'$ and $P_3'$.

In the following we will use the norms

$$\| \Theta \|_{1,\nu}^2 = \int_{X_{\nu-(1/2)}}^{X_{\nu+(1/2)}} | \Theta(X)|^2 \, dX$$

$$\| \Theta \|_{2,\nu}^2 = \int_{X_{\nu-(3/4)}}^{X_{\nu-(1/4)}} | \Theta(X)|^2 \, dX + \int_{X_{\nu+(1/4)}}^{X_{\nu+(3/4)}} | \Theta(X)|^2 \, dX.$$

From Eqs. (5) we get the following formula for $\phi'_{\nu,X2}$ and $\phi'_{\nu,X3}$.

$$\begin{aligned} \phi'_{\nu,X2} &= C_1(\bar{\phi}_{\nu+(1/2),X} - \bar{\phi}_{\nu-(1/2),X}) + C_2(\bar{\phi}_{\nu+(1/2),XX} + \bar{\phi}_{\nu-(1/2),XX}) \\ &\quad + C_3(\bar{\phi}_{\nu+(1/2),XXX} - \bar{\phi}_{\nu-(1/2),XXX}), \\ \xi \cdot \phi'_{\nu,X3} &= D_0(\bar{\phi}_{\nu+(1/2),0} - \bar{\phi}_{\nu-(1/2),0}) + D_1(\bar{\phi}_{\nu+(1/2),X} + \bar{\phi}_{\nu-(1/2),X}) \\ &\quad + D_2(\bar{\phi}_{\nu+(1/2),XX} - \bar{\phi}_{\nu-(1/2),XX}) + D_3(\bar{\phi}_{\nu+(1/2),XXX} + \bar{\phi}_{\nu-(1/2),XXX}), \end{aligned} \tag{6}$$

with

$$\begin{aligned} &C_1 = 1.5625; \quad C_2 = -0.28125; \quad C_3 = 0.03645833; \\ &D_0 = -8.63340304; \quad D_1 = 4.31670152; \quad D_2 = 0.22587392; \\ &D_3 = 0.02733791 \quad \text{for } \Delta X = 1. \end{aligned}$$

*Two Space Dimensions*

The equation of motion is again Eq. (1), but $\mathbf{r}$ is now a function of $X$ and $Y$. The grid $(X_\nu, Y_\mu)$ and the shifted grid $(X_\nu', Y_\mu') = (X_{\nu+(1/2)}, Y_{\mu+(1/2)})$ will be used. The notation will be the same as that used in the one-dimensional case. Only the periodic boundary case will be described, which means that all series $\alpha_{\nu,\mu}$ satisfy the requirement

$$\alpha_{\nu+L,\mu} = \alpha_{\nu,\mu} = \alpha_{\nu,\mu+L}.$$

Since we are dealing only with degree parameters 2 and 3, continuous fields are described by associating constants with the edges and sides of a grid square $(X_\nu, Y_\mu)$, $(X_{\nu+1}, Y_\mu)$, $(X_{\nu+1}, Y_{\mu+1})$, $(X_\nu, Y_{\mu+1})$ or $(X_{\nu+(1/2)}, Y_{\mu+(1/2)})$, $(X_{\nu+(3/2)}, Y_{\mu+(1/2)})$, $(X_{\nu+(3/2)}, Y_{\mu+(3/2)})$, $(X_{\nu+(1/2)}, Y_{\mu+(3/2)})$ in the shifted grid.

To define a function $\phi(X, Y) \in S_3$ let the constants $\phi_{\nu,\mu}$ ; $\phi_{\nu+(1/2),\mu,X2}$ ; $\phi_{\nu+(1/2),\mu,X3}$ ; $\phi_{\nu,\mu+(1/2),Y2}$ ; $\phi_{\nu,\mu+(1/2),Y3}$ be given. For $X \in [X_\nu, X_{\nu+1}]$ and $Y \in [Y_\mu, Y_{\mu+1}]$ we define

$$\begin{aligned}
\phi(X, Y) = &\left(\phi_{\nu,\mu+1}\frac{Y - Y_\mu}{\Delta X} + \phi_{\nu,\mu}\frac{Y_{\mu+1} - Y}{\Delta X}\right)\frac{X_{\nu+1} - X}{\Delta X} \\
&+ \left(\phi_{\nu+1,\mu+1}\frac{Y - Y_\mu}{\Delta X} + \phi_{\nu+1,\mu}\frac{Y_{\mu+1} - Y}{\Delta X}\right)\frac{X - X_\nu}{\Delta X} \\
&+ (\phi_{\nu+(1/2),\mu,X2}f_2(X - X_{\nu+(1/2)}) + \phi_{\nu+(1/2),\mu,X3} \\
&\cdot f_3(X - X_{\nu+(1/2)}))\frac{Y_{\mu+1} - Y}{\Delta X} \\
&+ (\phi_{\nu+(1/2),\mu+1,X2}f_2(X - X_{\nu+(1/2)}) + \phi_{\nu+(1/2),\mu+1,X3} \\
&\cdot f_3(X - X_{\nu+(1/2)}))\frac{Y - Y_\mu}{\Delta X} \\
&+ (\phi_{\nu,\mu+(1/2),Y2}f_2(Y - Y_{\mu+(1/2)}) + \phi_{\nu,\mu+(1/2),Y3} \\
&\cdot f_3(Y - Y_{\mu+(1/2)}))\frac{X_{\nu+1} - X}{\Delta X} \\
&+ (\phi_{\nu+1,\mu+(1/2),Y2}f_2(Y - Y_{\mu+(1/2)}) + \phi_{\nu+1,\mu+(1/2),Y3} \\
&\cdot f_3(Y - Y_{\mu+(1/2)}))\frac{X - X_\nu}{\Delta X}. \qquad (7)
\end{aligned}$$

The space $S_3'$ consists of all functions

$$\phi'(X, Y) = \phi(X + \Delta X/2, Y + \Delta X/2)$$

with $\phi \in S_3$. $\phi'$ is associated with a set of constants

$$\phi'_{\nu+(1/2),\mu+(1/2)} ; \quad \phi'_{\nu,\mu+(1/2),X2} ; \quad \phi'_{\nu,\mu+(1/2),X3} ;$$
$$\phi'_{\nu+(1/2),\mu,Y2} ; \quad \phi'_{\nu+(1/2),\mu,Y3} .$$

Figure 1 shows the definition of these constants in the grids.

For the definition of a function $\bar{\phi}(X, Y) \in P_3$ the constants $\bar{\phi}_0$, $\bar{\phi}_X$, $\bar{\phi}_Y$, $\bar{\phi}_{YX}$, $\bar{\phi}_{YY}$, $\bar{\phi}_{XX}$, $\bar{\phi}_{YYY}$, $\bar{\phi}_{YYX}$, $\bar{\phi}_{YXX}$, $\bar{\phi}_{XXX}$ must be given. The space index $\nu + (1/2)$, $\mu + (1/2)$ is dropped. For $X \in [X_\nu, X_{\nu+1}]$, $Y \in [Y_\mu, Y_{\mu+1}]$, $\phi$ is then defined by a spatial Taylor series

$$\begin{aligned}
\bar{\phi}(X, Y) = &\bar{\phi}_0 + \bar{\phi}_X(X - \bar{X}) + \bar{\phi}_Y(Y - \bar{Y}) \\
&+ \bar{\phi}_{XX}(X - \bar{X})^2/2 + \bar{\phi}_{YY}(Y - \bar{Y})^2/2 \\
&+ \bar{\phi}_{YX}(X - \bar{X})(Y - \bar{Y}) + \bar{\phi}_{YYX}(X - \bar{X})(Y - \bar{Y})^2/2 \\
&+ \bar{\phi}_{YXX}(X - \bar{X})^2(Y - \bar{Y})/2 + \bar{\phi}_{YYY}(Y - \bar{Y})^3/6 \\
&+ \bar{\phi}_{XXX}(X - \bar{X})^3/6, \qquad (8)
\end{aligned}$$

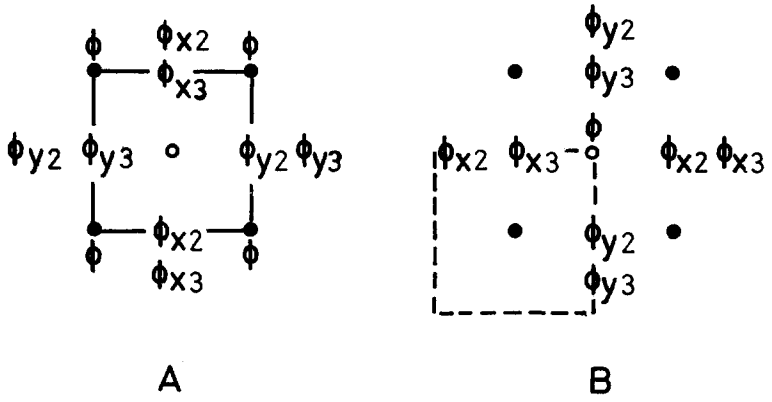


FIG. 1. Field representation in the original (A) and the shifted grid (B). ●, original gridpoints; ○, shifted gridpoints; ———, grid square of the original grid; – – – –, grid square of the shifted grid.

with $\bar{X} = X_{\nu+(1/2)}$ and $\bar{Y} = Y_{\mu+(1/2)}$. Functions $\bar{\phi}'(X, Y) \in P_3'$ are defined by

$$\phi'(X, Y) = \bar{\phi}(X + \Delta X/2, Y + \Delta X/2), \qquad \bar{\phi} \in P_3 .$$

The spaces $S_3$, $S_3'$, $P_3$, $P_3'$ are needed for the design of the third degree scheme. For the definition of the second degree scheme we will need the spaces $S_2$, $S_2'$, $P_2$, $P_2'$. The corresponding functions can be obtained by using Eqs. (7) with $\phi_{\nu+(1/2),\mu,X3} = \phi_{\nu,\mu+(1/2),Y3} = 0$ and Eqs. (8) with $\bar{\phi}_{\nu+(1/2),\mu+(1/2),XXX} = \bar{\phi}_{\nu+(1/2),\mu+(1/2),YYY} = \bar{\phi}_{\nu+(1/2),\mu+(1/2),YXX} = \bar{\phi}_{\nu+(1/2),\mu+(1/2),YYX} = 0$.

The time translation operator $T_{\Delta t}$ will now be defined on the space $B_A$ which consists of functions $\psi(X, Y)$. They are required to be periodic in the $X$ and $Y$ directions with periodicity length $L\Delta X$, and analytic except possibly at a finite number of lines. It is defined by

$$T_{\Delta t}\psi(X, Y) = \psi(X, Y) + \sum_{n=1}^{\rho} \psi^{(n)}(X, Y)(\Delta t^n/n!) \tag{9}$$

for the $\rho$th degree case. The coefficients $\psi^{(n)}$ are again determined by $\psi$ and Eq. (1).

The spatial smoothing operations $Q, Q'$ are mappings $P_3 \to S_3'$ and $P_3' \to S_3$, respectively. Their definition can be reduced to the case of one space dimension. For the definition of $Q$, let a function $\bar{\phi}(X, Y) \in P_3$ be given. Consider the function

$$\eta_{\mu+(1/2)}(X) = \bar{\phi}(X, Y_{\mu+(1/2)}).$$

The application of the one space dimensional smoothing operation will define the constants

$$\phi'_{\nu+(1/2),\mu+(1/2)} ; \qquad \phi'_{\nu,\mu+(1/2),X2} ; \qquad \phi'_{\nu,\mu+(1/2),X3} .$$

The smoothing of the function $\theta_{\nu+(1/2)}(Y) = \tilde{\phi}(X_{\nu+(1/2)}, Y)$ will give the constants $\phi'_{\nu+(1/2),\mu+(1/2)}$ ; $\phi'_{\nu+(1/2),\mu,Y2}$ ; $\phi'_{\nu+(1/2),\mu,Y3}$ which are sufficient to define a function $\phi'(X, Y) \in S_3'$. Note that no ambiguity occurs for the definition of $\phi'_{\nu+(1/2),\mu+(1/2)}$.

The spatial smoothing operations for the second degree case can be obtained by using Eqs. (6) with $C_3 = D_0 = D_1 = D_2 = D_3 = 0$.

*Blue Terms*

The definition of the time translation operator by Eqs. (4) and (9) requires a further simplification. Let a function $\psi$ from $S_\rho$ ($\rho \in \{2, 3\}$) be given. The functions $\psi^{(n)}$ defined by Eq. (4) or Eq. (9) are developed into a spatial Taylor series

$$\psi^{(n)} = \psi_0^{(n)} + \psi_X^{(n)}(X - X_{\nu+(1/2)}) + \cdots$$

or (10)

$$\psi^{(n)} = \psi_0^{(n)} + \psi_X^{(n)}(X - X_{\nu+(1/2)}) + \psi_{YX}^{(n)}(X - X_{\nu+(1/2)})(Y - Y_{\nu+(1/2)}) + \cdots$$

for one or two space dimensions, respectively.

Together with Eq. (4) or Eq. (9) one obtains a space–time Taylor series. The terms of higher than $\rho$th order will be called blue terms and are dropped in the following applications. For example, $\psi_X^{(2)}$ is a blue term for the second degree method, while for the third degree method it must be considered.

In one space dimension blue terms can only occur in the solution of nonlinear equations.

In two space dimensions the solution of the linear advection equation

$$(\partial/\partial t)\phi = -u_1(\partial\phi/\partial X) - u_2(\partial\phi/\partial Y)$$

with the second degree scheme contains the blue terms $\phi_{XX}^{(1)}$, $\phi_{YY}^{(1)}$, $\phi_{XY}^{(1)}$, $\phi_X^{(2)}$, $\phi_Y^{(2)}$. A numerical experiment has shown that their neglection has no noticeable effect on the solution when $\Delta t$ is small compared to the Courant–Levy timestep.

*Computational Procedure*

If the function $\phi^t \in S_\rho$ at time $t$ is given, the double timestep can be defined by

$$\phi^{t+2\Delta t} = Q' \circ T_{\Delta t} \circ Q \circ T_{\Delta t}\phi^t.$$

Consider the mapping $Q \circ T_{\Delta t}: S_\rho \to S_\rho'$ for the case $\rho = 3$ and one space dimension. Its computation is done in three steps. The spatial interpolation step

computes the spatial derivatives at $X_{\nu+(1/2)}$. From Eq. (2) we get the following interpolation formula (the time index $t$ is dropped).

$$\begin{aligned}
\bar{\phi}_{\nu+(1/2),0} &= (\phi_{\nu+1} + \phi_\nu)/2 - \phi_{\nu+(1/2)X2}\,\Delta X^2/8,\\
\bar{\phi}_{\nu+(1/2),X} &= (\phi_{\nu+1} - \phi_\nu)/\Delta X - \phi_{\nu+(1/2),X3}\cdot 1/24,\\
\bar{\phi}_{\nu+(1/2),XX} &= \phi_{\nu+(1/2),X2},\\
\bar{\phi}_{\nu+(1/2),XXX} &= \phi_{\nu+(1/2),X3}.
\end{aligned} \tag{11}$$

In the time translation step Eq. (4) is used to compute the fields at a later time level $t + \Delta t$. It is represented by a function $\bar{\phi}^{t+\Delta t} \in P_3$. From Eqs. (4) and (9) we get

$$\begin{aligned}
\bar{\phi}_0^{t+\Delta t} &= \bar{\phi}_0{}^t + \phi_0^{(1),t}\,\Delta t + \phi_0^{(2),t}\,\Delta t^2/2 + \phi_0^{(3),t}\,\Delta t^3/3,\\
\bar{\phi}_X^{t+\Delta t} &= \bar{\phi}_X{}^t + \phi_X^{(1),t}\,\Delta t + \phi_X^{(2),t}\,\Delta t^2/2,\\
\bar{\phi}_{XX}^{t+\Delta t} &= \bar{\phi}_{XX}^t + \phi_{XX}^{(1),t}\,\Delta t,\\
\bar{\phi}_{XXX}^{t+\Delta t} &= \bar{\phi}_{XXX}^t.
\end{aligned} \tag{12}$$

The space index $\nu + (1/2)$ was dropped and the blue terms were neglected in Eqs. (12).

The coefficients $\phi_0^{(1),t}$, $\phi_0^{(2),t}$, $\phi_0^{(3),t}$, $\phi_X^{(1),t}$, $\phi_X^{(2),t}$, $\phi_{XX}^{(1),t}$ are given for the case of the linear advection equation

$$(\partial/\partial t)\phi = (\partial/\partial X)\phi. \tag{13}$$

The space index $\nu + (1/2)$ and the time index $t$ will be dropped.

$$\begin{aligned}
\phi_0^{(1)} &= \bar{\phi}_X,\\
\phi_X^{(1)} &= \bar{\phi}_{XX},\\
\phi_{XX}^{(1)} &= \bar{\phi}_{XXX},\\
\phi_0^{(2)} &= \phi_X^{(1)},\\
\phi_X^{(2)} &= \phi_{XX}^{(1)},\\
\phi_0^{(3)} &= \phi_X^{(2)}.
\end{aligned} \tag{14}$$

Finally, the spatial smoothing step is performed according to Eqs. (6).

The neglect of the third order terms in Eqs. (6), (10), (11), (12), and (14) will give the computational procedure for the second degree case described in [1].

The two dimensional examples will be given for the second degree method. In this case, the interpolation step computes the spatial derivatives $\bar{\phi}_0$, $\bar{\phi}_X$, $\bar{\phi}_Y$, $\bar{\phi}_{YX}$, $\bar{\phi}_{YY}$, $\bar{\phi}_{XX}$ at the center $(X_{\nu+(1/2)}, Y_{\mu+(1/2)})$ of a grid square. The blue terms $\bar{\phi}_{YXX}$ and $\bar{\phi}_{YYX}$ are neglected. The time translation is done by using the mixed derivatives $\phi_0^{(1)}$, $\phi_X^{(1)}$, $\phi_Y^{(1)}$, $\phi_0^{(2)}$. A detailed description of the computational procedure for this case was given in [2], where the implementation of other than periodic boundary conditions is also described.

*The Demand for Computation Time*

The program for the physical instability case given in Section 3 needed 1.8 sec of computation time per time step on a CDC 3800. It may be interesting to see the demand of computation time required by the described methods in a nontrivial case.

We consider baroclinic six-layer meteorological models which use actual data as initial conditions. The models use the primitive Navier–Stokes equations in three space dimensions on a stereographic grid. The vertical acceleration is neglected. Horizontal discretization is done by the second and third degree methods respectively. In the vertical, the centered difference approximation is used. A description of the third degree model and its results is given in [5]. The vertical structure of the models is identical with that of a DWD model which uses an Eliassen grid. The models differ only with respect to their horizontal discretization and the computation area, which is quasi-hemispheric for the Eliassen-grid model and covers Europe and the Atlantic for the other two models. All models use $\Delta X = 381$ km.

The third degree model needs approximately as much computation time as an Eliassen-grid model of equal area with grid length $\Delta X/2$ would need. The transition from the third degree model to the second degree model reduces the computation time by one half. It should be remarked that the third degree model omits some of the third order terms. For example, the fields representing the stereographic mapping factor and the Coriolis parameter are given as function from $S_2$ instead of $S_3$.

The third degree model is economically competitive for short range prediction models if one accepts that it has an increased resolution compared with $\Delta X$-grid models. The effective grid length is $\Delta X' = \Delta X/3$, because in addition to grid point values of the fields it uses second and third spatial derivatives as degrees of freedom. While some of the additional resolution of the second degree method is lost by the smoothing of the $2\Delta X$ wave scale, it cannot be doubted that the third degree model actually has an increased resolution.

A detailed discussion of the resolution of the third degree method is given in [5]. In this paper the distinction is made between static and dynamic resolution. The first is given by the smallest scale which fields constant with time may have. The

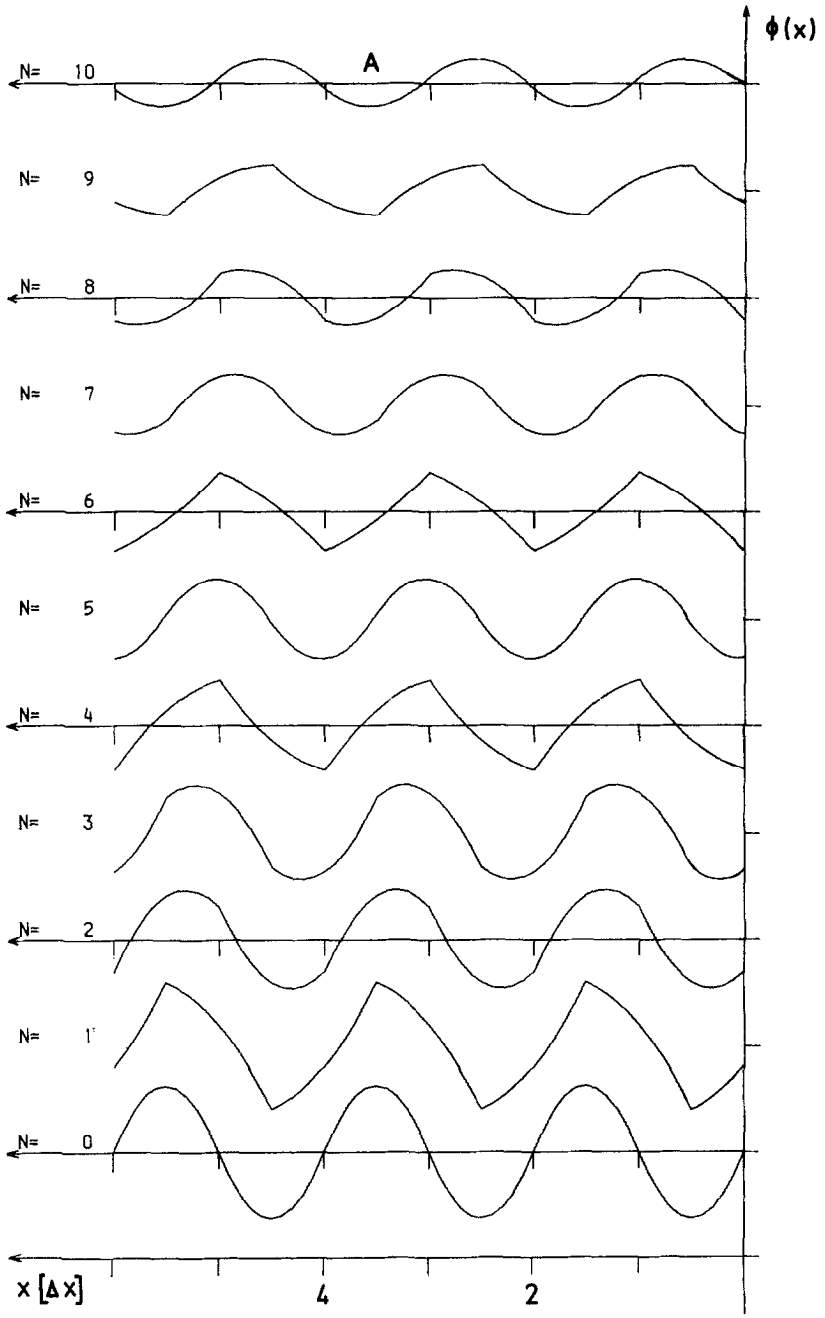


FIG. 2. The time development of the $2\Delta X$ wave. (A) Second degree method.

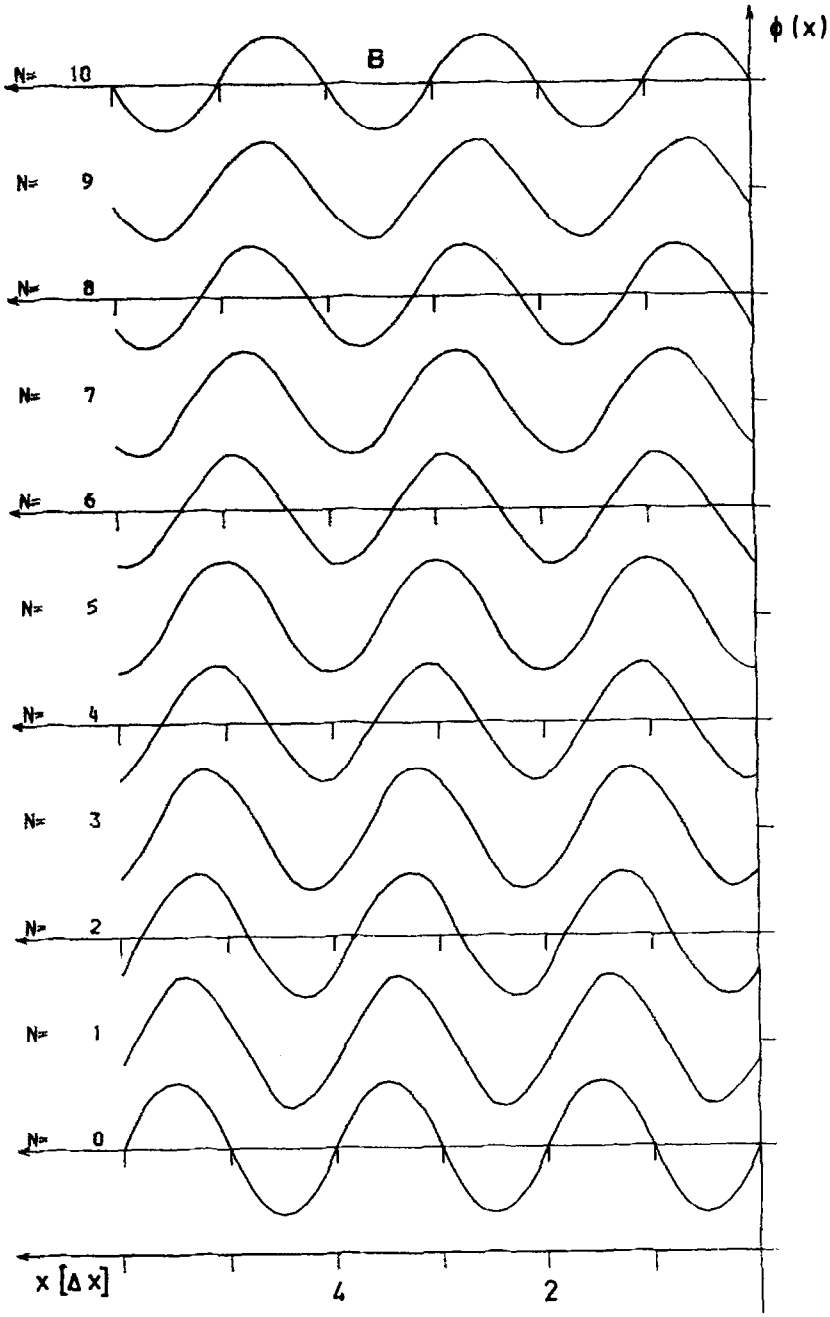


FIG. 2. (B) Third degree method.

second is given by the smallest scale which time dependant structures are allowed to have.

There is always less dynamic resolution than static resolution. For example, a scheme with grid length $\Delta X$ can represent a function with a jump on the scale $\Delta X$. However, it is not possible to predict a shock of this sharpness. According to comparative shock calculations with different methods [6], $3\Delta X$ seems to be a practical lower limit for the diameter of a shock.

The static resolution of the third degree method is that of a method with grid length $\Delta X' = \Delta X/3$. A third degree polynomial on the interval $[X_\nu, X_{\nu+1}]$ can equivalently be determined by prescribing $\phi_\nu$, $\phi_{\nu+(1/3)}$, $\phi_{\nu+(2/3)}$, $\phi_{\nu+1}$ instead of $\phi_\nu$, $(\partial^2/\partial X^2)\,\phi_{\nu+(1/2)}$, $(\partial^3/\partial X^3)\,\phi_{\nu+(1/2)}$, $\phi_{\nu+1}$. The dynamic resolution was determined in [5] by considering the sharpness of a predicted shock in comparison with predictions of other methods given in [6]. It was concluded that the third degree method has also the dynamic resolution of a scheme with grid length $\Delta X' = \Delta X/3$.

The Eliassen scheme used for comparison is one of the simpler methods used in meteorology. The schemes used for general circulation models and extended forecasts are much more time consuming because of their conservation properties and other reasons [5].

## 3. Computational Evidence

*Linear Advection Equation*

Now we put $\Delta X = 1$. The first example shows how the method uses its degrees of freedom to describe the field between the grid points. The linear advection equation (Eq. (13)) is solved by the third degree method with the initial condition

$$\phi_\nu = \phi_{\nu+(1/2),X_3} = 0, \qquad \phi_{\nu+(1/2),X_2} = A(-1)^\nu$$

with $\Delta t = 0.1$. Figure 2 shows the field for the first 10 timesteps as computed with the second and third degree methods.

The initial condition represents the $2\Delta X$ wave. The movement of this wave cannot be computed by methods which represent fields only by gridpoint values. This example shows that the transition to the second or third degree method produces an increase in resolution.

To investigate the numerical accuracy of the third degree scheme, wave solutions of the linear advection equation were considered. The initial conditions were

$$\begin{pmatrix} \phi_\nu^0 \\ \phi^0_{\nu+(1/2),X_2} \\ \phi^0_{\nu+(1/2),X_3} \end{pmatrix} = \begin{pmatrix} \alpha_1 \\ \alpha_2 \\ \alpha_3 \end{pmatrix} e^{i(2\pi/L)\nu}.$$

After $2n$ timesteps the field is given by

$$\begin{pmatrix} \phi_\nu^{2n} \\ \phi_{\nu+(1/2),X_2}^{2n} \\ \phi_{\nu+(1/2),X_3}^{2n} \end{pmatrix} = V^{2n} \begin{pmatrix} \phi_\nu^0 \\ \phi_{\nu+(1/2),X_2}^0 \\ \phi_{\nu+(1/2),X_3}^0 \end{pmatrix}.$$

The matrix $V$ and its eigenvalues $\lambda_1$, $\lambda_2$, $\lambda_3$ were computed numerically. The Courant–Levy condition for the third degree method is $\Delta t \leqslant 0.22\Delta X$. Figure 3 shows the damping factors $A^{n+1}/A^n$ and relative phase velocities $C/C_0$ corresponding to the first eigenvalue $\lambda_1$.

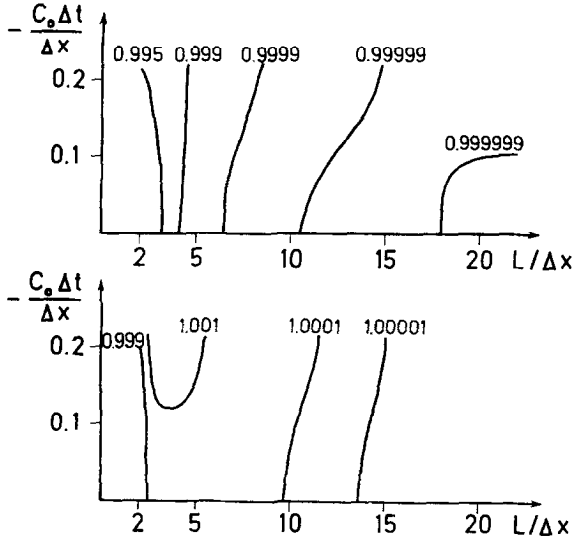


FIG. 3. Damping factors (above) and relative phase velocities (below) for the third degree method, corresponding to the first eigenvalue.

A comparison with [1] shows that the accuracy has improved considerably compared with the second degree method. The eigenvalues $\lambda_2$ and $\lambda_3$ represent modes with considerable damping. The damping factors are shown in Fig. 4.

These eigenvalues reflect the damping of small scale structures. Figure 5 shows two examples of these subgrid structures together with the result of one timestep ($\Delta t = 0$). The example below transforms the initial condition into a $2\Delta X$ wave in only one timestep.

To show the effect of the small damping and phase velocity error a computation with a positive initial condition was done. Periodic boundary conditions were

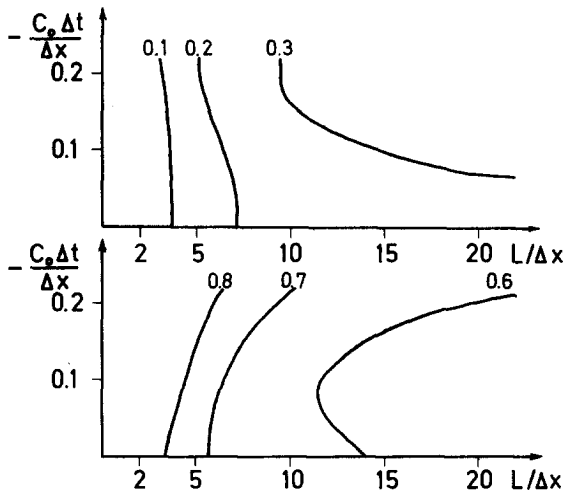


FIG. 4. The damping factors $A^{n+1}/A^n$ corresponding to the third and second eigenvalues.

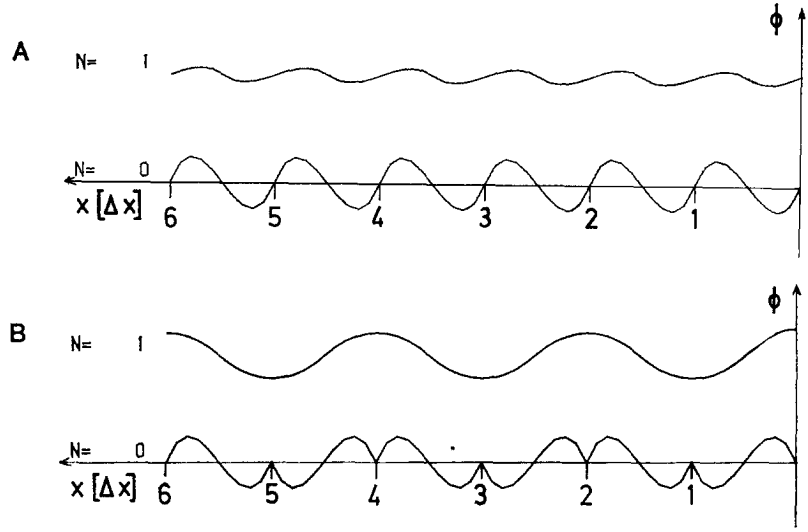


FIG. 5. Examples of subgrid structures with considerable damping. $N = 0$, initial condition; $N = 1$, result of one timestep with $\Delta t = 0$.

used with periodicity length $20\Delta X$ and $\Delta t = 0.1$. Figure 6 shows the result of forecasts. Except for $N = 2$ the forecast time was chosen in such a way that the exact solution of Eq. (13) would give the same diagram as the initial condition.

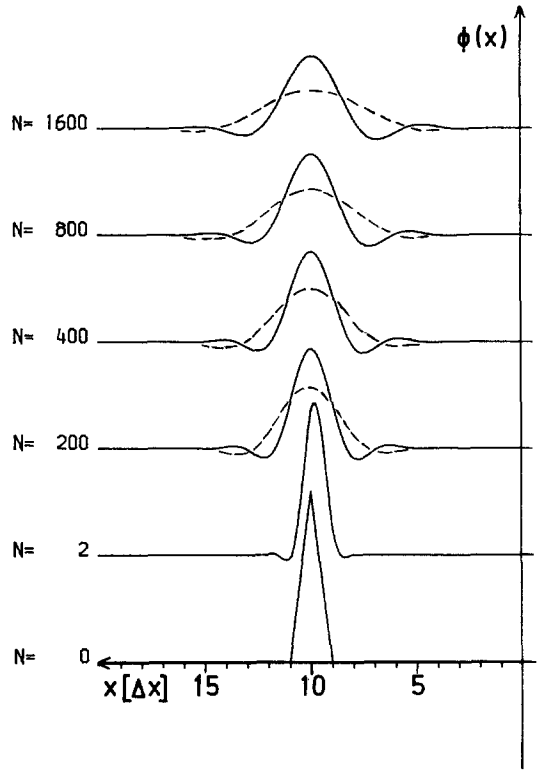


FIG. 6. Solution of the linear advection equation with positive initial values. $N$, number of timesteps; – – – –, second degree method; ———, third degree method.

*Vortex behind a Barrier*

The nonlinear computations were done with the equations of a barotropic fluid:

$$\begin{aligned}(\partial/\partial t)U &= -U(\partial U/\partial X) - V(\partial U/\partial Y) - (\partial H/\partial X),\\ (\partial/\partial t)V &= -U(\partial V/\partial X) - V(\partial V/\partial Y) - (\partial H/\partial Y),\\ (\partial/\partial t)H &= -(\partial(HU)/\partial X) - (\partial(HV)/\partial Y).\end{aligned} \tag{15}$$

It is a fluid with a free surface of height $H$ and only horizontal motion.

The computation was done with the second degree method on a $31 \times 31$ point grid with $\Delta X = 381$ km and $\Delta t = 1/12$ hr. The distance between the opposing boundaries was $29\Delta X$. Periodic boundary conditions were used in $X$-direction, and for $Y = Y_1$ and $Y = Y_2$ physically rigid boundaries were introduced. At $X = X_0 = 10\Delta X$ a physically rigid barrier of length $9\Delta X$ was introduced, which

was connected with one of the boundaries. The implementation of boundary conditions was done in the original grid. It was done two times, approaching the barrier from both sides. Correspondingly in the right grid the fields were double valued functions on the barrier. This reflects a jump discontinuity of the fields on this line. The initial values were

$$U = U_{00} = 190.5 \text{ km/hr}, \qquad V = 0, \qquad H = 2.0\ (381 \text{ km/hr})^2.$$

Figure 7 shows the velocity field after 21 hr. Figure 8 gives the total energy as a function of time. The dissipation first decreases and then increases again when the fully developed vortex reaches the barrier a second time.

The equations of motion (Eqs. (15)) describe no production of vorticity. In this example the spatial smoothing operation in combination with the boundary condition resulted in a production of vorticity in a physically reasonable way.

*Physical Instability*

The example above and the shock wave computation given in [2] already demonstrate the nonlinear stability of the second degree scheme in two space dimensions. A further nonlinear stability test was done by the computation of a physical unstable case.

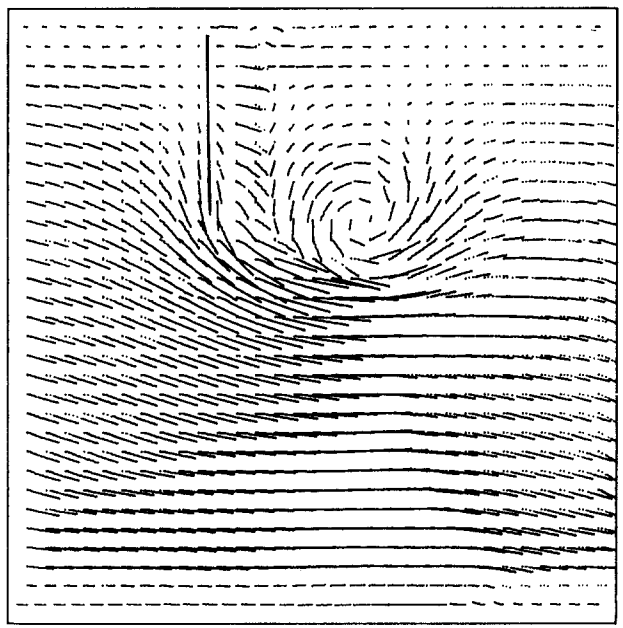

FIG. 7. The velocity field of the vortex behind a barrier at $t = 21$ hr.

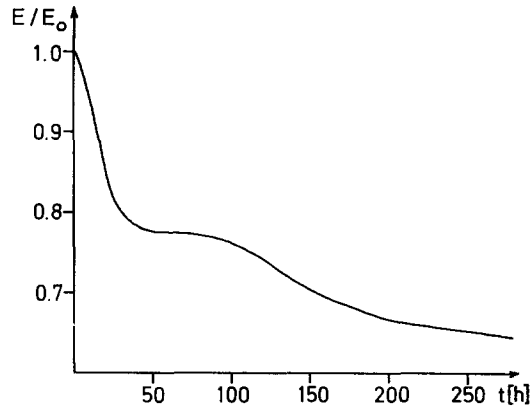


FIG. 8. The energy diagram of the vortex behind a barrier.

In case of turbulent motion, nature makes excessive use of its infinite number of degrees of freedom. According to [3] this situation poses a hard test for a finite difference scheme. The spatial smoothing operation of the second degree scheme will transform some motions into a larger scale and damp out other scales. In this way it maintains nonlinear stability.

The solution of the second degree method can be expected to be more stable than the exact solution. On the other hand, from the moderate damping of larger scales, one can expect that the computation actually represents the instability.

The example uses the equations of the barotropic fluid (Eqs. (15)). The computation with the second degree method was done on a $31 \times 31$ grid with $\Delta X = 381$ km and $\Delta t = 1/17$ hr. The distance of the opposing walls was $29\Delta X$. Periodic boundary conditions were used in the $X$-direction and at $Y = Y_1$ and $Y = Y_2$ we assume physically rigid boundaries.

The initial values were

$$\begin{aligned} H(X, Y) &= 2.0\,(381 \text{ km/hr})^2, \\ V(Y, X) &= 0, \\ U(Y, X) &= f(Y), \end{aligned} \tag{16}$$

with

$$\begin{aligned} f(Y) &= -1060 \text{ km/hr} \quad \text{for} \quad Y \leqslant 15\Delta X, \\ &= 0 \qquad\qquad\quad \text{for} \quad Y > 15\Delta X. \end{aligned} \tag{17}$$

For every choice of $f(Y)$, Eqs. (16) give stationary solutions both of the differential equations (Eqs. (15)) and of the finite difference equations.

There are, however, physical considerations [4] which show that the choice of $f(Y)$ given by Eqs. (17) produces a physically unstable boundary at $Y = 15\Delta X$.

Linear theory also proves the instability of this boundary. The computation resulted in a stationary flow with $f(Y)$ being submitted to the spatial smoothing operation. At $T = 46$ hr a small perturbation was introduced into the velocity field. Figure 9 shows the perturbed and unperturbed fields. During the computation the perturbation at first disappeared. At $t = 99$ hr small scale structures appeared in the $H$-field which were quickly increasing their amplitude. Figures 10 to 12 show the $H$-field at different times. Figures 13 and 14 give the velocity field minus basis current and the velocity field at time $t = 156$ hr to show the irregularity of

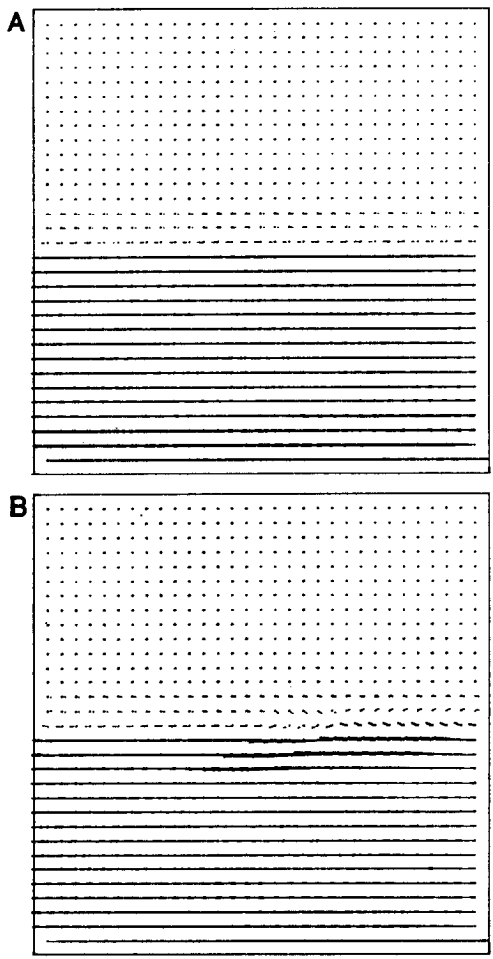


FIG. 9. The unperturbed (A) and the perturbed (B) state at $t = 46$ hr (physical instability).

FIGS. 10–12. The $H$-field at $t = 99$ hr, $t = 156$ hr, and $t = 456$ hr (physical instability).

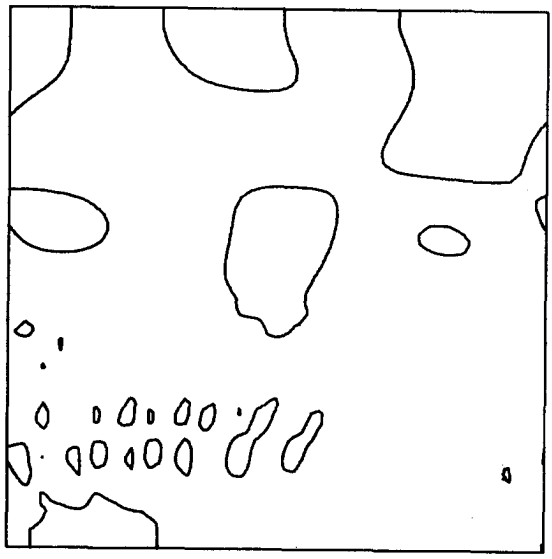

FIGURE 10

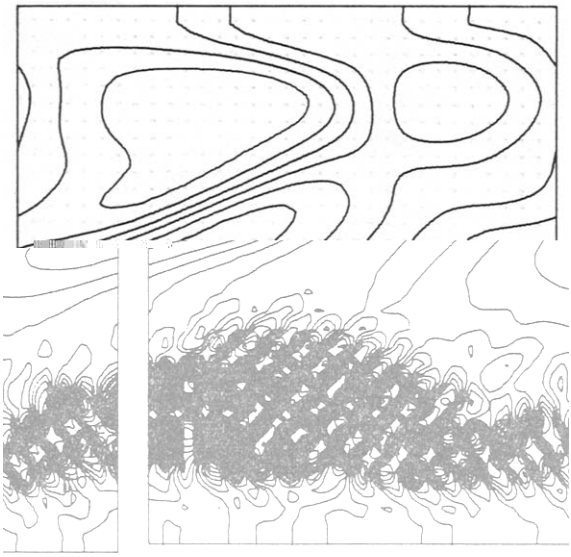

FIGURE 11

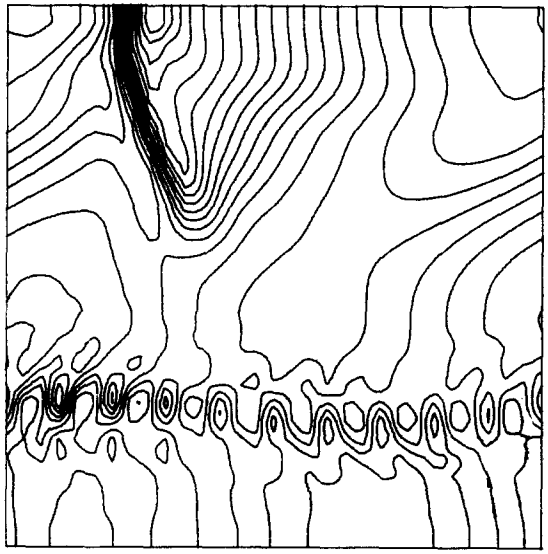

FIGURE 12

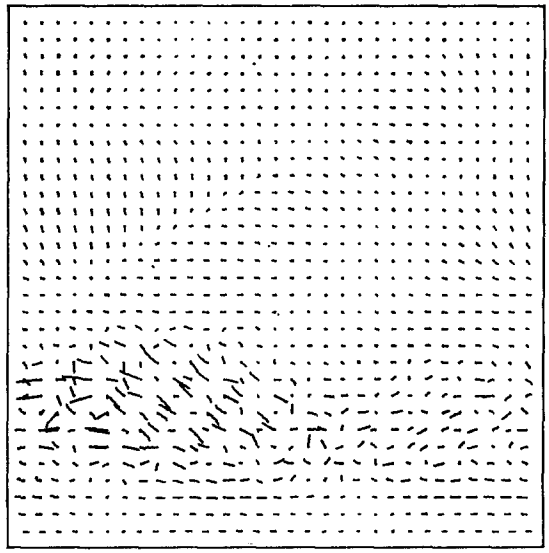

FIG. 13. Velocity field minus basis current at $t = 156$ hr (physical instability).

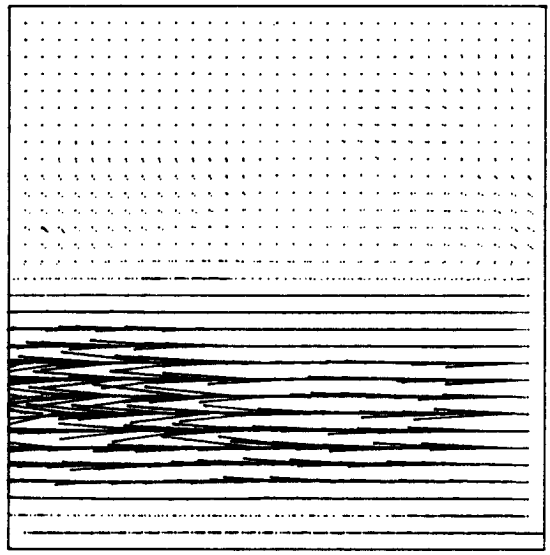

FIG. 14. Velocity field at $t = 156$ hr (physical instability).

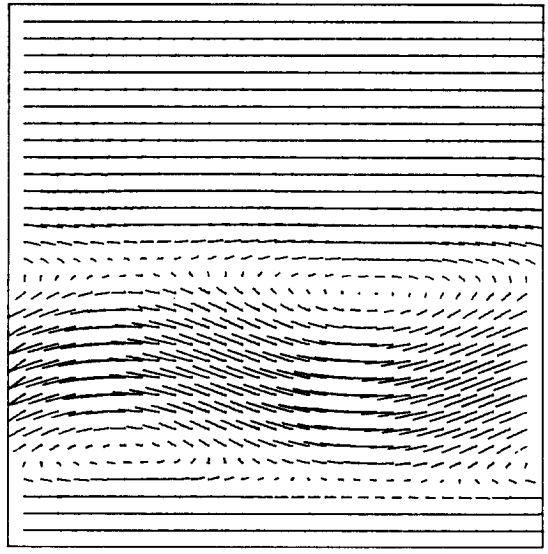

FIG. 15. The velocity field minus the field $U = 400$ km/hr, $V = 0$ at time $t = 1359$ hr (physical instability).

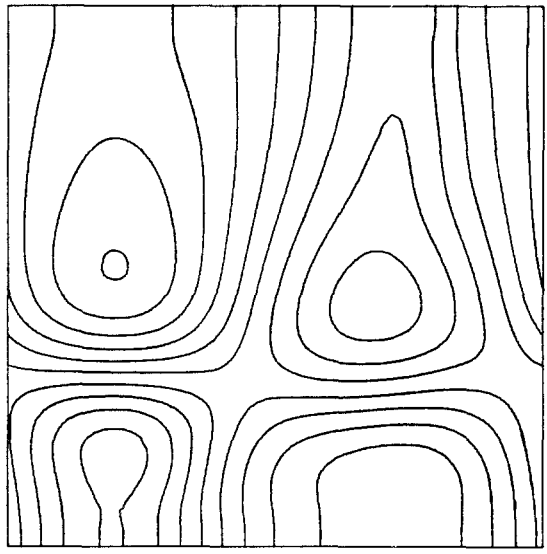

FIG. 16. The $H$-field corresponding to Fig. 15.

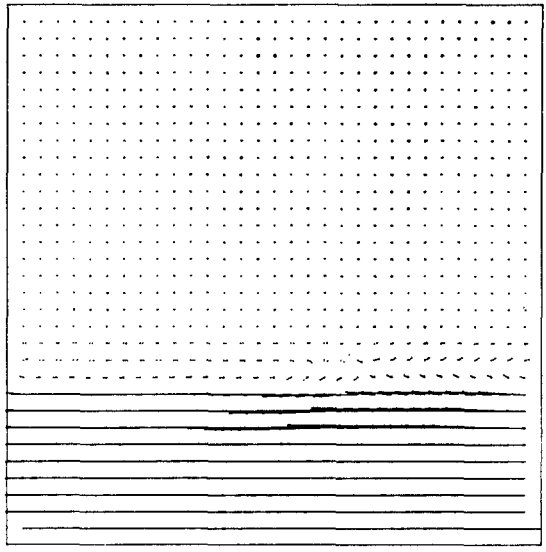

FIG. 17. The second initial condition after the introduction of the perturbation at $t = 46$ hr (physical instability).

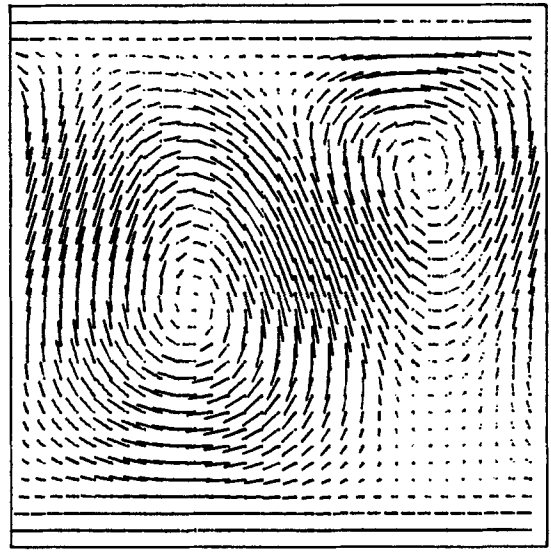

FIG. 18. The velocity field minus the field $U = 200$ km/hr, $V = 0$ at time $t = 473$ hr for the computation with the second initial condition (physical instability).

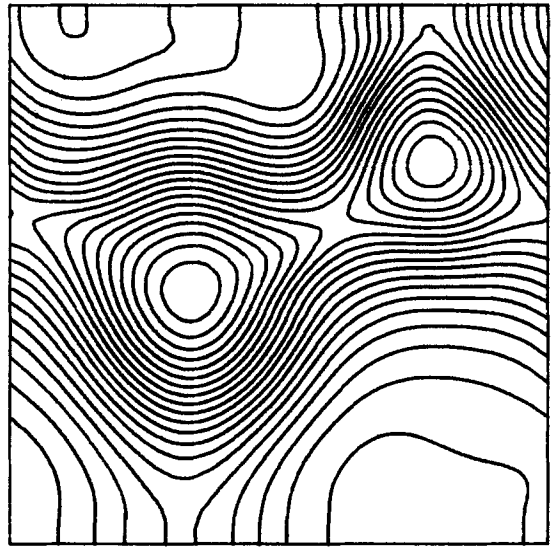

FIG. 19. The $H$-field corresponding to Fig. 18.

motion. The solution does not become numerically by unstable. The energy is decreasing and the total matter $\int H\,dX\,dY$ is conserved within 1%.

This property of the second degree scheme might be interesting for the computation of the large scale part of a flow with turbulent regions.

After the small scale movement has disappeared, a wave of a larger scale develops very slowly. Figure 15 shows the velocity field minus the field $U = 400$ km/hr, $V = 0$ at time $t = 1359$ hr. Figure 16 gives the corresponding $H$-field.

Another computation was done with a second initial condition representing a smaller flow region. Figure 17 gives the field at time $t = 46$ hr after the introduction of the perturbation.

The details of the resulting development are quite different compared with the result of the first initial condition. The small scale movement of the initial phase is very weak. The large scale wave develops more quickly and has a larger amplitude. Figure 18 shows the velocity field minus the field $U = 200$ km/hr, $V = 0$ at time $t = 473$ hr. Figure 19 gives the corresponding $H$-field. The system of two vortices has quite a different shape compared with Fig. 16. The relation of the distances of the vortices in $X$- and $Y$-direction is, however, approximately the same in both cases. It is not very different from the value corresponding to a stable Kárman vortex street [4].

When the computation was stopped, the development had not ended, although it was very slow. The energy was continuing to decrease at this time.

## ACKNOWLEDGMENTS

The author thanks J. Pfaendtner and W. Edelmann for their comments on the manuscript, and members of the Max-Planck-Institut für Strömungsforschung, Göttingen, for remarks on the physical instability case.

## REFERENCES

1. J. STEPPELER, *J. Computational Phys.* **19** (1975), 390.
2. J. STEPPELER, *Beitr. Phys. Atm.* **48** (1975), 278.
3. R. D. RICHTMEYER, *in* "Proceedings of the Third International Conference on Numerical Mehods in Fluid Mechanics," Vol. 1, p. 82, Springer–Verlag, Berlin/Heidelberg/New York, 1973.
4. L. PRANDTL, "Führer durch die Strömungslehre," Vieweg, Braunschweig, 1965.
5. J. STEPPELER, "A Baroclinic Model Using a High Accuracy Horizontal Discretization," to appear.
6. K. SRINIVAS, J. GURURAJA, AND K. K. PRASAD, *J. Computational Phys.* **20** (1976), 140.